

Article

A Six-Switch Mode Decoupled Wireless Power Transfer System with Dynamic Parameter Self-Adaption

Wei Wu^{1,2}, Daqing Luo^{1,*} , Jianfeng Hong³ , Zhe Tang¹ and Wenxiang Chen¹ 

¹ Department of Instrumental and Electrical Engineering, Xiamen University, Xiamen 361005, China; wuwei233@hotmail.com (W.W.); 35120211151591@stu.xmu.edu.cn (Z.T.); wxchen@xmu.edu.cn (W.C.)

² School of Mechanical & Electrical Engineering, Guizhou Normal University, Guiyang 550025, China

³ School of Mechanical and Automotive Engineering, Xiamen University of Technology, Xiamen 361005, China; hjf156@sina.com

* Correspondence: daqingluo_del@163.com; Tel.: +86-18695050050

Abstract: For the fully resonant wireless power transfer (WPT) system, the high coupling of the converter and the resonant network introduced many problems, such as frequency splitting, the power curve peak limit, and the strict switch strategy. To solve these problems, this paper proposed a new six-switch topology based on the full-bridge converter. With the unique structures containing two capacitor-isolated switches and a source-isolated diode, the system decouples the converter and the resonant network, and its modes have been decoupled, called the independent power injection and free resonance WPT (IPIFR-WPT) system. The capacitor-isolated switches and the source-isolated diode make the converter operate only when the voltage on the primary capacitor is equal to the source voltage, and the source will be isolated by the diode when the capacitor voltage is great than the source, which provides a wide time margin for the switches of the converter to turn on in advance. In this margin, the operation point is self-determined the same whenever the switches turn on so that the system's performance is consistent. Based on this characteristic, the system can self-adapt a dynamic change in system parameters, with at least 15% tolerance for the coupling coefficient and 14% for the load resistance.

Keywords: wireless power transfer; power injection; soft switching; parameter change; decouple



Citation: Wu, W.; Luo, D.; Hong, J.; Tang, Z.; Chen, W. A Six-Switch Mode Decoupled Wireless Power Transfer System with Dynamic Parameter Self-Adaption. *Electronics* **2023**, *12*, 2314. <https://doi.org/10.3390/electronics12102314>

Academic Editor: Fabio Corti

Received: 26 March 2023

Revised: 15 May 2023

Accepted: 17 May 2023

Published: 20 May 2023



Copyright: © 2023 by the authors. Licensee MDPI, Basel, Switzerland. This article is an open access article distributed under the terms and conditions of the Creative Commons Attribution (CC BY) license (<https://creativecommons.org/licenses/by/4.0/>).

1. Introduction

Wireless power transfer (WPT) technology uses electromagnetic fields for contactless power transfer [1]. Because there is no direct physical connection, it has higher security and better flexibility than traditional wired power transfer [2]. Therefore, WPT technology has developed very fast in recent years, especially on movable and rotatable devices, such as robots, electric vehicles, underwater devices, portable applications and implantable medical equipment [3–7].

The fully resonant wireless power transfer (FR-WPT) system has attracted the widest research in recent decades [8]. Due to the high coupling of the converter and the compensation network, FR-WPT systems really require the converter's switching frequency to be equal to the fixed frequency of the resonant network to achieve stable and efficient operation. Since the converter is fully coupled with the resonant network, the FR-WPT system has faced some issues, such as the power peak limit, the parameter change sensitivity, frequency splitting, and so on [9–11]. To solve these issues, some closed-loop strategies including impedance matching and frequency tracking are proposed to improve the dynamic performance and ensure the system's stable operation [12–15]. However, due to the limitation of the system's structure, the closed-loop strategy is limited by the power peak limit. Furthermore, because of the frequency splitting phenomenon, it is easy to fall into local solutions and even make the system unstable, causing irreversible damage to the device [16].

The independent power injection and free resonance wireless power transfer (IPIFR–WPT) system uses a novel and unique topology structure that separates the switching converters from the resonant tanks [17,18]. The characteristic of this circuit structure is that the power injection process and the free resonance process are independent so that the converter and the resonance network are completely decoupled. In the IPIFR–WPT system, the power injection process is completely controlled independently, and the free resonance is also completely independent. This control strategy's advantage is isolating the converter from the system and making the resonant network conduct passive-free resonance. Therefore, the frequencies of the converter and the resonant network are different, decoupling the resonant network and the converter, and simplifying the power control strategy [19]. At the same time, the operating frequency of the resonant network is also free to adapt to the influence of the change in the working parameters because it does not have to be affected by the operation of the converter, which solves the issues of frequency splitting and frequency tracking in the system.

Article [20] proposes a pulsed power injection IPIFR–WPT system. The principle is mainly to control the power injected into the coil inductance by controlling the turn-on time of the switch S_1 . However, the system requires precise control for switch S_2 , and its switching times must be strictly aligned with the zero crossing point of the resonant current. Otherwise, the soft switching condition will not be satisfied. This shortcoming causes strong adhesion between the converter and the resonance network, fails to achieve complete decoupling, has high requirements for the accuracy of the control system, is sensitive to parameter changes, and needs better dynamic performance. Article [21] proposes a full-bridge IPIFR–WPT system with six switches. The switches are used to periodically connect or isolate the resonant capacitor and the DC power supply into or out of the system to achieve power injection and free resonant mode switching. The single-switch IPIFR–WPT system uses only one switch to control mode switching, greatly reducing system switching losses and improving system efficiency [22,23]. The energy of the injection system can be adjusted by controlling the turn-on time of the switch to achieve the regulation of power, but the injection time cannot be too large. Furthermore, it is necessary to ensure that the current flowing through the primary inductor can be less than zero during the resonance process. Therefore, there is a theoretical power peak for the single-switch IPIFR–WPT system, which means the system cannot achieve wide-range power regulation.

Furthermore, a comparison of the technologies to improve the dynamic performance of the WPT system is summarized in Table 1. Normally, for the impedance matching method, a lot of components are used to adjust the equivalent input impedance [14]. Hence, the impedance matching method leads to the higher cost and larger size of the system. Moreover, the actual dynamic performance is discrete and approximate. Articles [15,16] use different frequency tracking methods to improve dynamic performance and eliminate frequency splitting. However, the high sensibility to the parameters needs precise design. Article [20] changes the structure of the converters to achieve the decoupling between the converter and the compensation network. However, the decoupling is incomplete, and the system is sensitive to the parameters.

In this paper, based on the traditional bridge circuit, a six-switch IPIFR–WPT system is proposed. Its unique capacitor-isolated switches and power-source-isolated diode mean the power supply and parallel resonant capacitor can be periodically connected or isolated from the system. When the power supply is connected to the system and the resonant capacitor is isolated, it is in the power injection mode. The longer the power injection mode duration, the more power is injected into the system. When the resonant capacitor is connected to the system and the power supply is isolated, the resonant network will use the energy stored in the inductance and capacitor to conduct free resonance. The resonant frequency is the fixed frequency of the resonant network and does not need to be controlled by the switches. Therefore, the six-switch IPIFR–WPT system realizes the mode decoupling of power injection and free resonance and the decoupling of the converter and resonant network. In addition, due to the source-isolated diode, the power supply can only inject

energy into the system in one direction. Thus, the switches have been turned on in advance to ensure that the power supply will not be connected to the system in advance, only when the voltage on the primary resonant capacitor drops to equal the power supply voltage, and the leading time range is relatively wide, which is called the soft switching margin. At the same time, the parasitic diode on the switch can ensure the zero voltage switching (ZVS) condition.

Table 1. Comparison of the technologies to improve dynamic performance.

Ref.	Dynamic Performance Improving Strategy	Inductors/Capacitors/ Switches on the Converter	Have Any Voltage/Current Sensors?	Control Strategy	Achieve Decoupling?	Sensibility to the Parameters
[14]	Impedance matching with a capacitor matrix	$1/(M \times N)/(M \times N + 1)$	Yes	Close loop	No	Low
[15]	Frequency tuning loops	1/1/4	Yes	Close loop	No	High
[16]	Maximum power point tracking	1/1/4	Yes	Close loop	No	High
[20]	Switch-mode adjusting	2/3/2	No	Open loop	Partially	High
Proposed	Power injecting structure	1/1/6	No	Open loop	Yes	Low

2. Circuit Structure and Mode Analysis

2.1. Circuit Structure and Mode Analysis

The prototype of the six-switch IPIFR–WPT system is shown in Figure 1. In Figure 1, a unidirectional power supply comprises an isolation diode D_0 and a DC power supply E_{dc} . The purpose of a one-way power supply is to ensure that energy entering the system does not return to the power supply. Switches S_1 – S_4 form a full-bridge converter to connect power E_{dc} to the system and inject energy into the system. Switches S_5 and S_6 let the primary compensation capacitor C_p be isolated from or connected to the system. Diodes D_1 – D_6 are the bypass diodes of switches S_1 – S_6 , wherein bypass diodes D_1 – D_4 do not function during the entire working process due to their different directions from isolation diode D_0 ; the bypass diodes D_5 and D_6 are used for continuous current conduction during the resonance process and can isolate C_p from the system. The self-inductances of the primary and secondary coils are L_p and L_s , while M is the mutual inductance of the coils. R_p and R_s are the parasitic resistance of the primary and secondary coils, respectively. The load R_0 consumes the energy received by the secondary circuit after being rectified by the back-end rectifying circuit of the secondary circuit. Supposing the inductive characteristics and the voltage drop of the back-end rectifier circuit are ignored, in that case, the equivalent load R_L can be used to convert the load resistance R_0 to the input terminal of the rectifier circuit, and the conversion relationship is as follows:

$$R_L = \frac{8R_0}{\pi^2}. \quad (1)$$

Figure 2 is the schematic diagrams of the operation modes of the six-switch IPIFR–WPT system. When the system operates, there are eight operating modes. Mode 1 connects the power supply E_{dc} to the system in a forward direction, a forward power injection mode. Modes 2–4 are resonant modes, also called free resonance processes, due to the isolation of the power supply E_{dc} from the system. Note that Modes 2 and 4 are transitional modes, both of which are unidirectional resonance processes. According to the symmetry of the full-bridge converter operation, Mode 5 reversely connects the power supply E_{dc} to the system as a reverse power injection mode. Furthermore, Modes 6–8 are resonant processes opposite to the working processes of Modes 2–4.

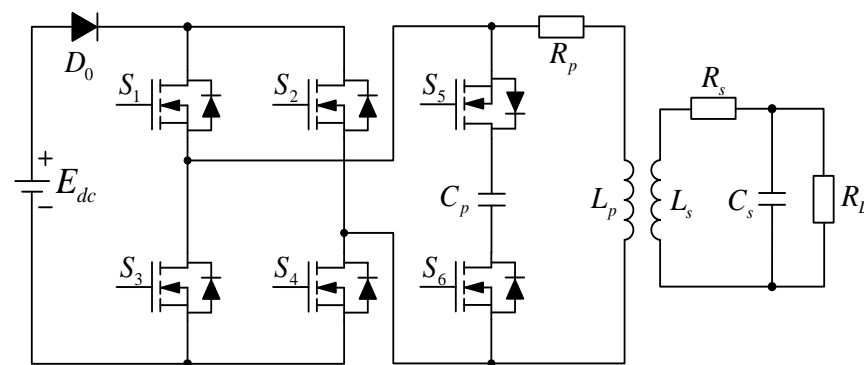


Figure 1. The topology of the six-switch IPIFR system.

Figure 3 shows the waveform diagram of the source current i_1 , the primary capacitor voltage u_p , and the primary inductor current i_p of the six-switch IPIFR–WPT system under steady-state operation. According to Figures 2 and 3, the operation modes of the six-switch IPIFR–WPT system can be analyzed as follows:

Mode 1 [t_0, t_1]: This is a forward power injection mode with a duration of $\zeta_1 = t_1 - t_0$. Before the time t_0 , the switches S_1 and S_4 have been turned on in advance, and the switches S_2 and S_3 remain turned off. At this time, the primary capacitor voltage u_p is greater than E_{dc} , forcing D_0 to be turned off, isolating the power supply E_{dc} from the system, thereby preventing the energy from being injected into the system. Until the time t_0 , the voltage u_p drops to equal to E_{dc} , causing diode D_0 to turn on, and the current i_p flows from the branch D_0 – C_p – S_5 to the switches S_1 and S_4 that have been turned on in advance. During the period [t_0, t_1], while the primary capacitor C_p is isolated from the system, the DC power supply E_{dc} directly injects energy into the primary inductor L_p .

Mode 2 [t_1, t_2]: This is a transitional mode of the first free resonance process. At the moment t_1 , the switches S_1 and S_4 turn off, and at the same time, the current i_p will continuously conduct through the bypass diode D_6 . At this time, the turning off of switches S_1 and S_4 meets the ZVS condition. In Mode 2, the primary inductor L_p and the primary compensation capacitor C_p form a resonant cavity and begin passive free resonance. The duration of Mode 2 is very short and can generally be taken as 1–2 μs , even a few hundred nanoseconds.

Mode 3 [t_2, t_3]: This is a bidirectional free resonant mode. Since the switch S_6 turns on at t_2 , the primary current i_p can achieve bidirectional free resonance in the resonant network L_p – C_p . During Mode 3, after the value of the current i_p resonates to less than zero, the flow direction of i_p in the branch is S_5 – C_p – S_6 . After that, at time t_3 , the switch S_5 turns off, and the current i_p can still continuously conduct through the bypass diode D_5 . The switch S_5 turns off to meet the ZVS condition. At the same time, at t_3 , the switches S_2 and S_3 turn on. Due to the capacitance voltage u_p being less than $-E_{dc}$ at this time, the isolation diode cannot be turned on, and the current cannot be exchanged from the branch D_5 – C_p – S_6 to the switches S_2 and S_3 . That is, before and after the turn-on of S_2 and S_3 , the current flowing through them is zero, satisfying the zero current switching (ZCS) condition.

Mode 4 [t_3, t_4]: In this mode, the system remains in a state of free resonance. In addition, the current i_p continuously conducts through the branch D_5 – C_p – S_6 during the time span until the time of t_4 , when the value of u_p rises to equal to $-E_{dc}$ through resonance. At time t_4 , because the switches S_2 and S_3 have turned on in advance at t_3 , the current i_p can be naturally switched from the branch D_5 – C_p – S_6 to the switches S_2 and S_3 , thereby switching to Mode 5.

Mode 5 [t_4, t_5]: This is a reverse power injection mode, which is reversed with Mode 1. Due to the natural commutation of the current i_p from the branch D_5 – C_p – S_6 to the switches S_2 and S_3 that have turned on before t_4 , the power supply E_{dc} is reversely connected to the system and injects energy into the primary inductor L_p .

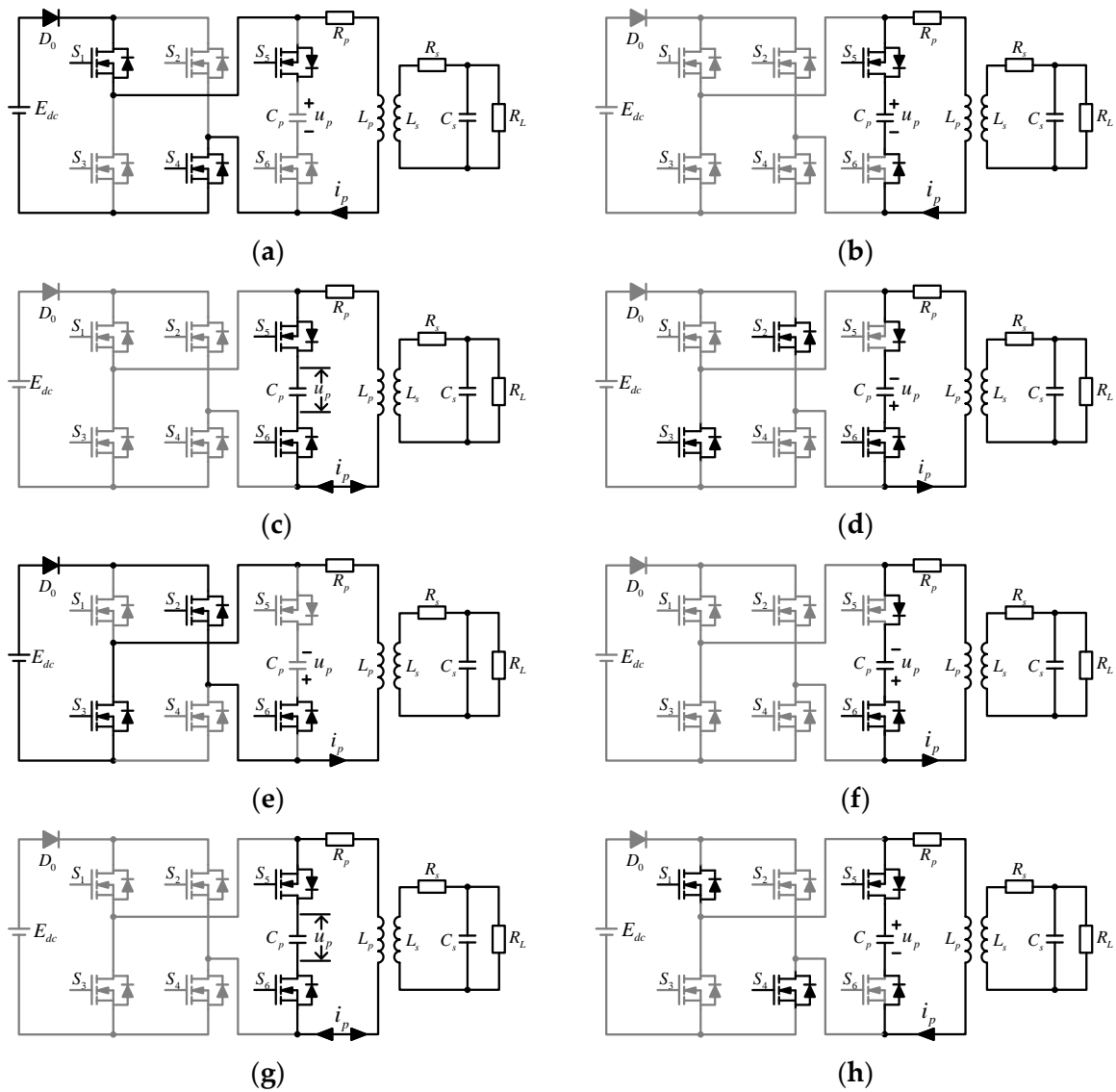


Figure 2. The operation mode diagram of the six-switch IPIFR–WPT system: (a) Mode 1, (b) Mode 2, (c) Mode 3, (d) Mode 4, (e) Mode 5, (f) Mode 6, (g) Mode 7, and (h) Mode 8.

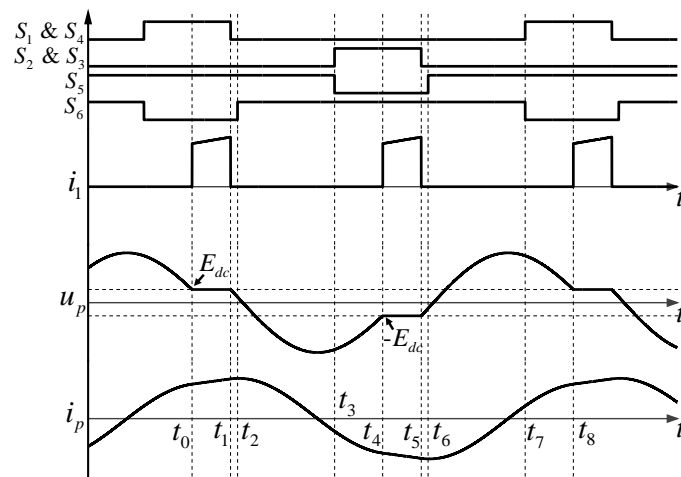


Figure 3. The steady-state operation waves of the six-switch IPIFR–WPT system.

Mode 6 [t_5, t_6]: This is a transitional mode of the second free resonance process, which is symmetric to Mode 2 and has a short duration. At time t_5 , the switches S_2 and S_3 turn off. Since the current i_p will be continuously conducted through the bypass diode D_5 , turning off switches S_2 and S_3 meets the ZVS condition. In Mode 6, the primary inductor L_p and the primary compensation capacitor C_p form a resonant network and begin free resonance.

Mode 7 [t_6, t_7]: This is a bidirectional free resonant mode symmetric to Mode 3. At t_6 , the switch S_5 turns on. Due to the capacitance voltage u_p greater than E_{dc} , the current i_p continuously conduct through the bypass diode D_5 without commutation to S_1 and S_4 . Therefore, the turn-on of switch S_5 satisfies the ZVS condition. Then the primary current i_p can achieve bidirectional free resonance in the resonant network L_p - C_p during [t_6, t_7].

Mode 8 [t_7, t_8]: This is a transitional mode symmetric to Mode 4. At t_7 , switch S_6 turns off while turning on switches S_1 and S_4 . Because of the voltage u_p being greater than E_{dc} , D_0 is turned off, and the current i_p continuously conducts through D_6 without commutation to S_1 and S_4 . Therefore, S_6 meets the ZVS condition, while the opening of S_1 and S_4 satisfies the ZCS condition. The resonant network maintains resonance during [t_7, t_8]. Until t_8 , the voltage u_p is equal to E_{dc} , and the current i_p naturally commutates from the resonant network to S_1 and S_4 . Meanwhile, the system operates into Mode 1.

2.2. Calculation of System Soft Switching Operating Point

Based on the mode analysis of the six-switch IPIFR-WPT system in the previous section, the switching conditions for its eight operation modes are shown in Figure 4. The eight operation modes of a six-switch IPIFR-WPT circuit can be classified as four cyclic operating processes, namely, the forward power injection process, the first free resonance process, the reverse power injection process, and the second free resonance process. Among them, Mode 1 and Mode 5 are forward and reverse power injection processes, respectively. Modes 2, 3, and 4 jointly constitute the first free resonance process, and Modes 6, 7, and 8 jointly constitute the second free resonance process.

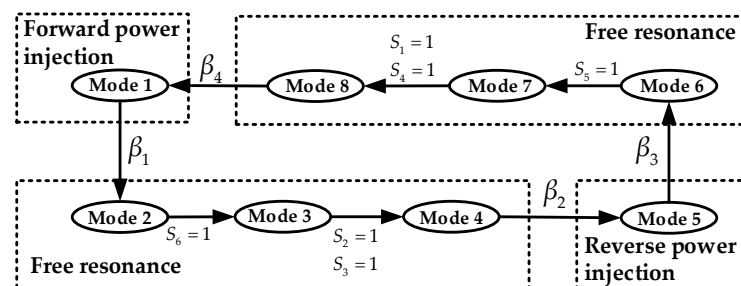


Figure 4. The diagram of mode switching boundaries.

Figure 4 shows no switch operates when the free resonance process switches to the power injection process. The switching condition is to rely on the voltage u_p to form a voltage clamp with the power supply voltage E_{dc} through the diode D_0 . In Mode 8, the switch groups S_1 and S_4 have turned on, but at this time, the voltage u_p is greater than E_{dc} , and the system remains in the free resonance process. Meanwhile, $i_p > 0$, that is, u_p will continue to decrease until u_p drops to equal to E_{dc} , and the diode D_0 reaches the critical conduction condition. At the same time, the current is commutated from branch S_6 - C_p - S_5 to branch S_4 - E_{dc} - D_0 - S_1 . The system switches from a free resonance process to a forward power injection process, and the voltage u_p on the primary capacitor C_p will maintain the voltage clamp at E_{dc} . Similarly, when switching from Mode 4 to Mode 5, it is necessary to clamp the voltage u_p on the primary capacitor C_p to $-E_{dc}$, and the free resonance process completes the switching to the reverse power injection process.

For convenience, the switching conditions $\beta_1, \beta_2, \beta_3$, and β_4 between the four operation processes are shown in Figure 4 and written in parallel:

1. β_1 : $S_1 = 0$ and $S_4 = 0$;
2. β_2 : $u_p = -E_{dc}$ and $i_p < 0$;
3. β_3 : $S_2 = 0$ and $S_3 = 0$;
4. β_4 : $u_p = E_{dc}$ and $i_p > 0$.

Figure 5 shows the equivalent circuit diagram of the main operation process of the six-switch IPIFR–WPT system. Since the state space model of the system during the forward power injection process and the reverse power injection process are entirely consistent, the equivalent circuit model is shown in Figure 5a. However, the bus voltages during the forward power injection and reverse power injection processes are different due to the conduction switch sets of the full-bridge converters, and their input voltages are E_{dc} and $-E_{dc}$, respectively. At the same time, the system models for the first and second free resonance processes are also entirely consistent, with their equivalent circuit models shown in Figure 5b, and there is no power input in the free resonance process.

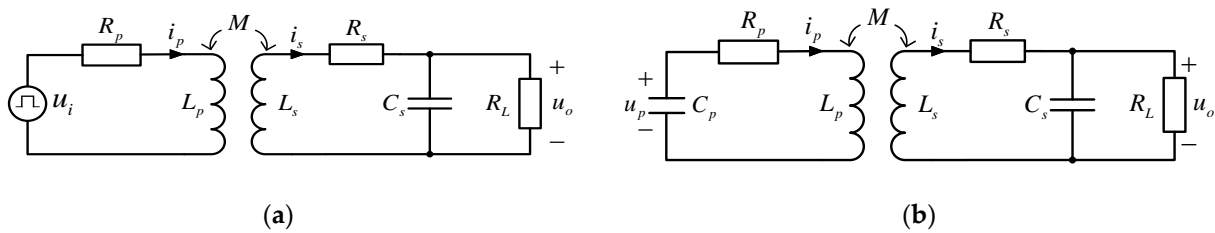


Figure 5. The equivalent circuits of the operation processes of the six-switch IPIFR–WPT system: (a) power injection process and (b) self-resonance process.

During the power injection process in Figure 5a, the primary compensation capacitor C_p is isolated from the system by the switches S_5 and S_6 being turned off. The DC power supply directly charges the primary inductance L_p through full-bridge forward conduction (switches S_1 and S_4) or reverse conduction (switches S_2 and S_3), with input voltages of E_{dc} or $-E_{dc}$, respectively. At the same time, due to the isolation diode D_0 , the current i_1 only flows in one direction, $i_1 > 0$, and energy can only be injected into the system from the power source and cannot be returned to the power source. In the free resonance process shown in Figure 5b, the DC power source is isolated from the system, while the inductance L_p and capacitance C_p in the primary circuit are directly connected to form a resonance circuit. Hence, through mutual inductance coupling, electrical power is transferred from the primary circuit to the secondary circuit.

According to Figure 5, set the state variable as the voltage u_p on the primary capacitor C_p , the current i_p on the primary coil inductance L_p , the current i_s on the secondary coil inductance L_s , and the voltage u_o on the secondary capacitor C_s , that is, $x = [u_p, i_p, i_s, u_o]^T$. Because the secondary capacitance C_s and the equivalent load resistance R_L are in parallel, the voltage u_o can also be considered as the equivalent output voltage. Assuming the system input is $u = [E_{dc}]$, differential equations can be listed as follows for each state variable according to Kirchhoff’s voltage law and current law:

Forward power injection process:

$$\dot{x} = A_1x + B_1u, \tag{2}$$

First free resonance process:

$$\dot{x} = A_2x, \tag{3}$$

Reverse power injection process:

$$\dot{x} = A_3x + B_3u, \tag{4}$$

Second free resonance process:

$$\dot{x} = A_4x, \tag{5}$$

where

$$A_1 = A_3 = \begin{bmatrix} 0 & 0 & 0 & 0 \\ 0 & \frac{L_s R_p}{\Delta} & \frac{M R_s}{\Delta} & \frac{M}{\Delta} \\ 0 & \frac{M R_p}{\Delta} & \frac{L_p R_s}{\Delta} & \frac{L_p}{\Delta} \\ 0 & 0 & \frac{1}{C_s} & -\frac{1}{C_s R_L} \end{bmatrix}, \tag{6}$$

$$B_1 = -B_3 = \begin{bmatrix} 0 & -\frac{L_s}{\Delta} & \frac{-M}{\Delta} & 0 \end{bmatrix}^T, \tag{7}$$

$$A_2 = A_4 = \begin{bmatrix} 0 & -\frac{1}{C_s} & 0 & 0 \\ -\frac{L_s}{\Delta} & \frac{L_s R_p}{\Delta} & \frac{M R_s}{\Delta} & \frac{M}{\Delta} \\ -\frac{M}{\Delta} & \frac{M R_p}{\Delta} & \frac{L_p R_s}{\Delta} & \frac{L_p}{\Delta} \\ 0 & 0 & \frac{1}{C_s} & -\frac{1}{C_s R_L} \end{bmatrix}, \tag{8}$$

$$\Delta = M^2 - L_p L_s, \tag{9}$$

$$M = k \sqrt{L_p L_s}. \tag{10}$$

For a linear time-invariant system $\Sigma: (A, B, C, D)$, if the system matrix A is invertible, and when the initial time is t_0 , the corresponding time domain solution can be expressed as follows [24]:

$$x(t) = x_{zi}(t) + x_{zt}(t) = \Phi(t - t_0)x_0 + A^{-1}[\Phi(t - t_0) - I]Bu, \tag{11}$$

where $\Phi(t) = \exp\{At\}$, I is the identity matrix, $x_{zi}(t)$ is the zero input response, $x_{zt}(t)$ is the zero state response, and x_0 is the initial state of the system at the initial time t_0 .

Since the system matrices A_1 and A_3 of the power injection process are irreversible, it is impossible to bring them into Equation (11) directly. Furthermore, the voltage u_p on the primary capacitor C_p is clamped at E_{dc} during the power injection process. Hence, the differential equation of u_p can be rewritten as follows:

$$\frac{du_p}{dt} = -u_p + E_{dc} \equiv 0. \tag{12}$$

Note that Equations (2) and (3) only hold during the power injection process. The system matrices A_1, A_3 and input matrices B_1, B_3 of the power injection process will be rewritten to be reversible as follows:

$$A_1 = A_3 = \begin{bmatrix} -1 & 0 & 0 & 0 \\ 0 & \frac{L_s R_p}{\Delta} & \frac{M R_s}{\Delta} & \frac{M}{\Delta} \\ 0 & \frac{M R_p}{\Delta} & \frac{L_p R_s}{\Delta} & \frac{L_p}{\Delta} \\ 0 & 0 & \frac{1}{C_s} & -\frac{1}{C_s R_L} \end{bmatrix}, \tag{13}$$

$$B_1 = -B_3 = \begin{bmatrix} 1 & -\frac{L_s}{\Delta} & \frac{-M}{\Delta} & 0 \end{bmatrix}^T. \tag{14}$$

According to Equation (11), if the initial state of the four linear time-invariant systems at their respective initial time t_0 is x_0 , the time domain solutions of the subsystems can be expressed as follows:

Forward power injection process:

$$x(t) = \Phi_1(t - t_0)x_0 + A_1^{-1}[\Phi_1(t - t_0) - I]B_1 E_{dc}, \tag{15}$$

First free resonance process:

$$x(t) = \Phi_2(t - t_0)x_0, \tag{16}$$

Reverse power injection process:

$$x(t) = \Phi_3(t - t_0)x_0 + A_3^{-1}[\Phi_3(t - t_0) - I]B_3E_{dc}, \tag{17}$$

Second free resonance process:

$$x(t) = \Phi_4(t - t_0)x_0. \tag{18}$$

Due to the symmetry of the two energy resonance processes and the two free resonance processes, the time interval experienced by their subsystems is the same, so the time interval between the two power injection processes is assumed to be ξ_1 . Set the time interval between two power injection processes as ξ_2 . Let the initial value of the system in the n th cycle be x_n , and the terminal values of the four subsystems be x_{n1} , x_{n2} , x_{n3} , and x_{n+1} , respectively, where x_{n+1} is the terminal value of the system in the n th cycle and also the initial value of the system in the $(n + 1)$ cycle. The expressions for the terminal values x_{n1} , x_{n2} , x_{n3} , and x_{n+1} of each subsystem are as follows:

$$x_{n1} = \Phi_1(\xi_1)x_n + A_1^{-1}[\Phi_1(\xi_1) - I]B_1E_{dc}, \tag{19}$$

$$x_{n2} = \Phi_2(\xi_2)x_{n1}, \tag{20}$$

$$x_{n3} = \Phi_3(\xi_1)x_{n2} + A_3^{-1}[\Phi_3(\xi_1) - I]B_3E_{dc}, \tag{21}$$

$$x_{n+1} = \Phi_4(\xi_2)x_{n3}. \tag{22}$$

According to the modal analysis and the symmetry of the full-bridge system, when the system's operating state reaches a steady state, there is $x_n = -x_{n2} = x_{n+1}$. Generally, $x_n = x_{n+1}$ is called a fixed point, and the mapping relationship between x_n and x_{n+1} becomes a fixed point mapping. To simplify the iterative process, take $x_n = -x_{n2}$ for fixed point mapping calculations, and the following equation can be obtained:

$$x_n = -x_{n2} = -\Phi_2(\xi_2)\Phi_1(\xi_1)x_n - \Phi_2(\xi_2)A_1^{-1}[\Phi_1(\xi_1) - I]B_1E_{dc}. \tag{23}$$

After transforming and bringing $\xi_2 = 1/2T - \xi_1$ for Equation (23), we can obtain the following equation:

$$x_n = -[I + \Phi_2(\frac{1}{2}T - \xi_1)\Phi_1(\xi_1)]^{-1} \Phi_2(\frac{1}{2}T - \xi_1)A_1^{-1}[\Phi_1(\xi_1) - I]B_1E_{dc}. \tag{24}$$

According to the modal analysis and subsystem switching conditions, the initial value of the system needs to meet the boundary $\beta_4.u_p = E_{dc}$ and $i_p > 0$. Namely, the element up in the fixed point x_n is constant, and the following equation can be expressed:

$$-C_1[I + \Phi_2(\frac{1}{2}T - \xi_1)\Phi_1(\xi_1)]^{-1} \Phi_2(\frac{1}{2}T - \xi_1)A_1^{-1}[\Phi_1(\xi_1) - I]B_1E_{dc} = E_{dc}. \tag{25}$$

Therefore, the soft switching operation point of the six-switch IPIFR-WPT system is the solution of Equation (25), and we can construct the following function $g(\xi_1)$ to solve Equation (25):

$$g(\xi_1) = 1 + C_1[I + \Phi_2(\frac{1}{2}T - \xi_1)\Phi_1(\xi_1)]^{-1} \Phi_2(\frac{1}{2}T - \xi_1)A_1^{-1}[\Phi_1(\xi_1) - I]B_1. \tag{26}$$

The parameters of the six-switch IPIFR–WPT system are shown in Table 2. The curve of the function $g(\xi_1)$ with $T = 110 \mu\text{s}$ is shown in Figure 6. There are two results of $g(\xi_1) = 0$, that is, $\xi_{1a} = 11.11 \mu\text{s}$ and $\xi_{1b} = 36.02 \mu\text{s}$. Then, we bring ξ_{1a} and ξ_{1b} into (20) to solve the corresponding fixed point x_n , listed in Table 3.

Table 2. The main parameters of the six-switch IPIFR–WPT system.

Parameter	Value	Parameter	Value
L_p	660 μH	E_{dc}	100 V
L_s	585 μH	k	0.5
R_p, R_s	0.2 Ω	R_L	10 Ω
C_p, C_s	0.4 μF	T	110 μs

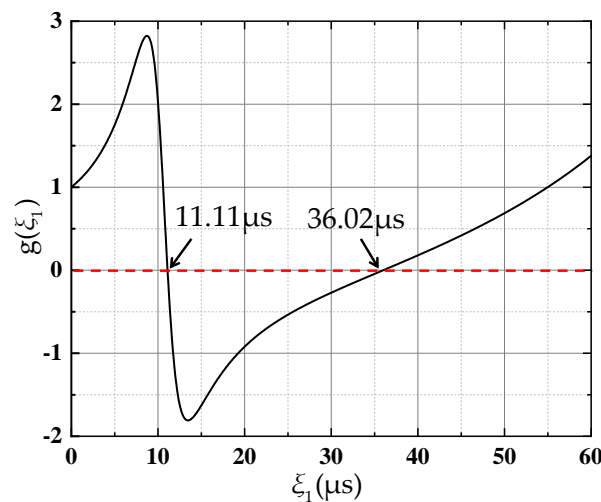


Figure 6. The curve of the function $g(\xi_1)$ with respect to ξ_1 .

Table 3. The calculated result of the fixed point x_n and the intermediate variable x_{n1} .

Operation Point	x_n				x_{n1}			
	u_p (V)	i_p (A)	i_s (A)	u_o (A)	u_p (V)	i_p (A)	i_s (A)	u_o (A)
11.11 μs	100.0	9.812	5.986	56.594	100.0	11.305	5.657	57.483
36.02 μs	100.0	−3.273	−1.260	−17.146	100.0	3.850	2.287	20.212

The fixed point x_n is both the initial and final values of the steady-state period. Moreover, the fixed point x_n must satisfy the boundary condition β_4 ($u_p = E_{dc}$ and $i_p > 0$). In Table 3, when taking $\xi_{1a} = 11.11 \mu\text{s}$, the value of fixed point x_n satisfies the boundary condition β_4 , and when taking $\xi_{1b} = 36.02 \mu\text{s}$, $i_p = -3.272 \text{ A} < 0$ does not meet the boundary condition β_4 . Therefore, the root $\xi_{1b} = 36.02 \mu\text{s}$ could be abandoned ($x_n = -x_{n2} = x_{n+1}$).

After calculating the fixed point x_n and the transition state quantity x_{n1} of the six-switch IPIFR–WPT system, according to the proposed symmetry of the full-bridge converter, there are $x_n = -x_{n2} = x_{n+1}$, $x_{n1} = -x_{n3}$. Then, in order to more intuitively represent the trade-off between the two results mentioned above, by substituting x_n and x_{n1} obtained in Table 3 into Equations (19)–(22), the curves of state variables in the complete steady-state cycle can be obtained, and the curves of current i_p and voltage u_p in them can be plotted in Figure 7.

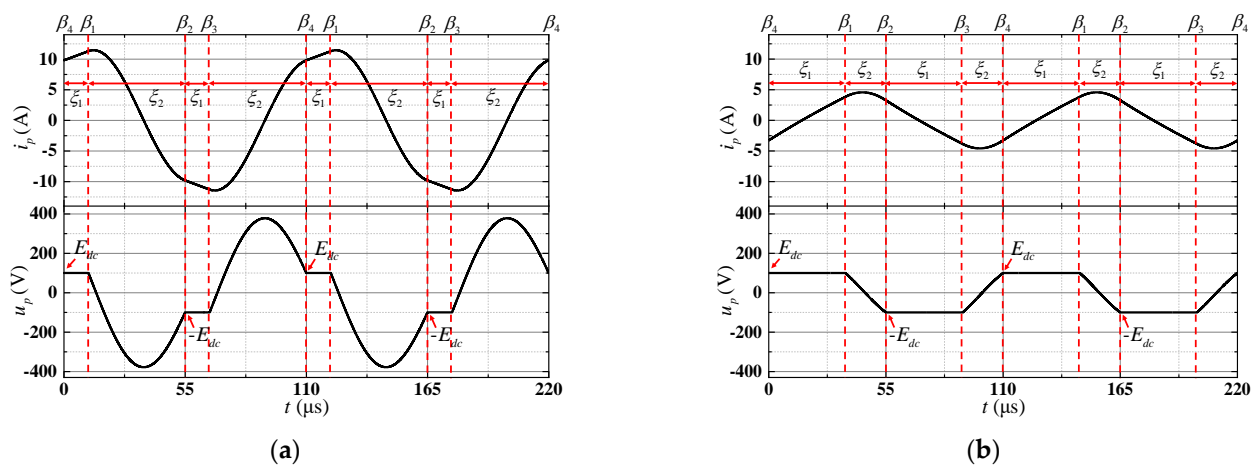


Figure 7. The waves of system state variables under the calculated steady-state operation points: (a) $\zeta_1 = 11.11 \mu\text{s}$ and (b) $\zeta_1 = 36.02 \mu\text{s}$.

As can be seen from Figure 7, taking $\zeta_{1a} = 11.11 \mu\text{s}$, the simulation waveform is consistent with the mode analysis, and all boundary conditions can be satisfied within a steady-state cycle. However, taking $\zeta_{1b} = 36.02 \mu\text{s}$, the calculated operating waveform is inconsistent with the expected, and the boundary conditions β_2 ($u_p = -E_{dc}$ and $i_p < 0$) and β_4 ($u_p = E_{dc}$ and $i_p > 0$) cannot be satisfied, so that ζ_{1b} can be abandoned.

3. System Characteristics and Experimental Results

3.1. Experimental Devices

In order to verify the characteristics of the six-switch IPIFR–WPT system, an experimental platform was built, as shown in Figure 8. As shown in Figure 8a, the DC power supply used in the system consists of three parts: an AC voltage regulator TDGC2–3kVA (Delixi, China), a single-phase rectifier module MDQ100A1600V, and a filter capacitor. The oscilloscope is RTB2004, produced by Rohde & Schwarz Company. The power analyzer is the WT500, produced by Yokogawa Company. The resonance capacitors C_s and C_p are MKPH–R 0.4 μF . In Figure 8b, the isolation diode D_0 used in the system is FR607 (1000 V, 6 A) and the switches S_1 – S_6 are IXFN56N90P (900 V, 56 A).

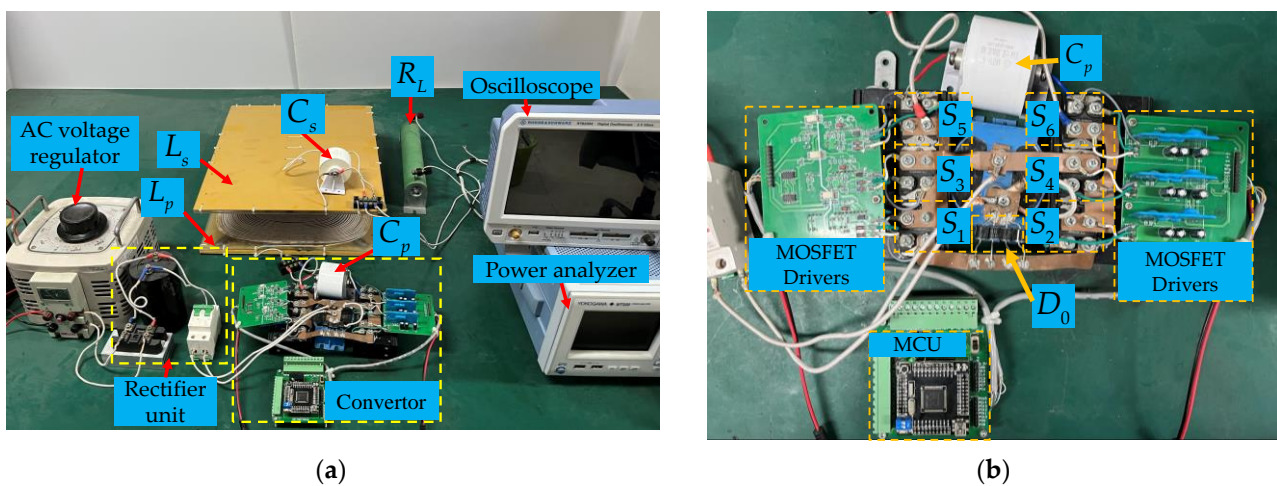


Figure 8. Experimental devices of the six-switch IPIFR–WPT system: (a) the whole system and (b) the converter.

The square coupling coils used in this system use litz wires while using a radial layout of ferrite to increase their self-inductances and mutual inductance. The size of the square

coils is 32 cm times 40 cm. The self-inductances L_p and L_s of the primary and secondary coils are 660 μH and 585 μH , respectively. The internal resistances R_p and R_s are both 0.2 Ω . The relationship between the coupling coefficient k and the coil distance d is shown in Figure 9.

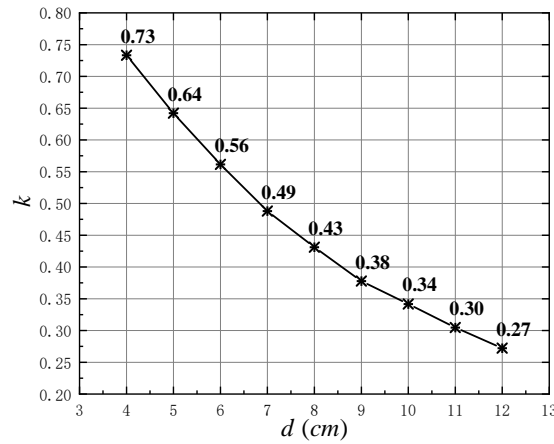


Figure 9. The relationship between the coupling coefficient k and coil distance d of the flat coils.

3.2. Soft Switching Margin Characteristic

The six-switch IPIFR-WPT system has a unique wide soft switching margin characteristic due to its particular structure. In Mode 4 and Mode 8, the last modes of the free resonance process, the full-bridge converter has been turned on in advance, but the voltage u_p is greater than E_{dc} so that the diode D_0 is turned off and the power supply is isolated from the system. Since the free resonance process will maintain until the voltage u_p is equal to E_{dc} , the switches of the full-bridge converter could turn on before in a very time margin when the voltage u_p is greater than E_{dc} . Hence, in this time margin, the system itself will achieve the soft switching condition and determine the operation point without any switching action. The time margin is called the soft switching margin.

Figure 10 is a schematic diagram of the wide soft switching margin of a six-switch WPT system. In Figure 10, the black curve is the voltage input of the full-bridge converter, and the orange and red curves represent the values of the primary capacitor voltage u_p and the primary inductor current i_p , respectively.

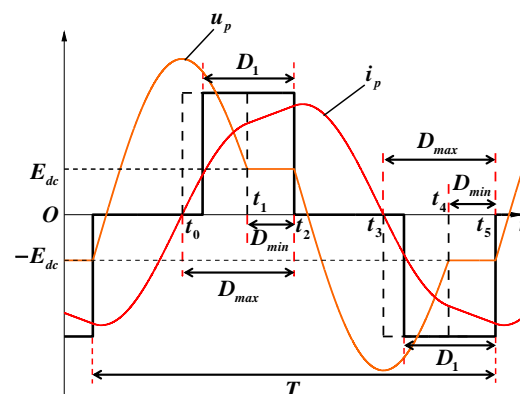


Figure 10. The diagram of the wide soft switching margin of the six-switch IPIFR-WPT system.

According to the modal analysis above, boundary conditions must be met when switching from the second free resonance process to the forward power injection process β_4 ($u_p = E_{dc}$ and $i_p > 0$), and switches S_1 and S_4 have been turned on in advance. It can be known from the waveforms of voltage u_p and current i_p in Figure 10 that the timing of turn-on of S_1 and S_4 must meet the following conditions: $u_p > E_{dc}$ and $i_p > 0$. Therefore, the margin

that satisfies the soft switching condition is $[t_0, t_1]$. Namely, the maximum pulse width for S_1 and S_4 is $D_{max} = t_2 - t_0$, and the minimum opening pulse width is $D_{min} = t_2 - t_1$. Based on the symmetry of the full-bridge converter, there are $D_{max} = t_5 - t_3 = t_2 - t_0$ and $D_{min} = t_5 - t_4 = t_2 - t_1$. The pulse widths of switch groups (S_1, S_4) and (S_2, S_3) can meet the conditions by taking any value of $[D_{min}, D_{max}]$. Therefore, the time range $[D_{min}, D_{max}]$ can be called the wide soft switching margin of a six-switch IPIRF-WPT system, and M_{ZVS} is defined as the wide soft switching margin of the system, and its calculation formula is as follows:

$$M_{ZVS} = \frac{D_{max} - D_{min}}{T} \times 100\% \tag{27}$$

In Figure 11a–c, let the fixed coil spacing be $d = 6$ cm ($k \approx 0.5$), the equivalent load resistance be $R_L = 10 \Omega$, and the period be $T = 110 \mu\text{s}$. Then, taking the positive pulse widths of the switching strategy as (a) $D = 15 \mu\text{s}$, (b) $D = 20 \mu\text{s}$, and (c) $D = 26 \mu\text{s}$, the system can self-determine the same operating point, $\zeta_1 = 10.52 \mu\text{s}$, very close to the theoretical value, $\zeta_1 = 11.11 \mu\text{s}$. Meanwhile, the waveform shape and amplitude of the capacitor voltage u_p and the inductor current i_p are consistent. According to the measurement results in Figure 11, the soft switching margin under the above static parameters is $D_{min} = 10.52 \mu\text{s}$ to $D_{max} = 29.95 \mu\text{s}$. In Figure 11, the three positive pulse widths of (a), (b), and (c) are all within the range of $[D_{min}, D_{max}]$ and can enable the system to operate at the same operating point and meet soft switching conditions. Therefore, it can be proven that the unique topology of the six-switch IPIRF-WPT system enables it to have a wide soft switching margin, which provides a wide tolerance for the control system, improves system stability, and reduces control difficulty.

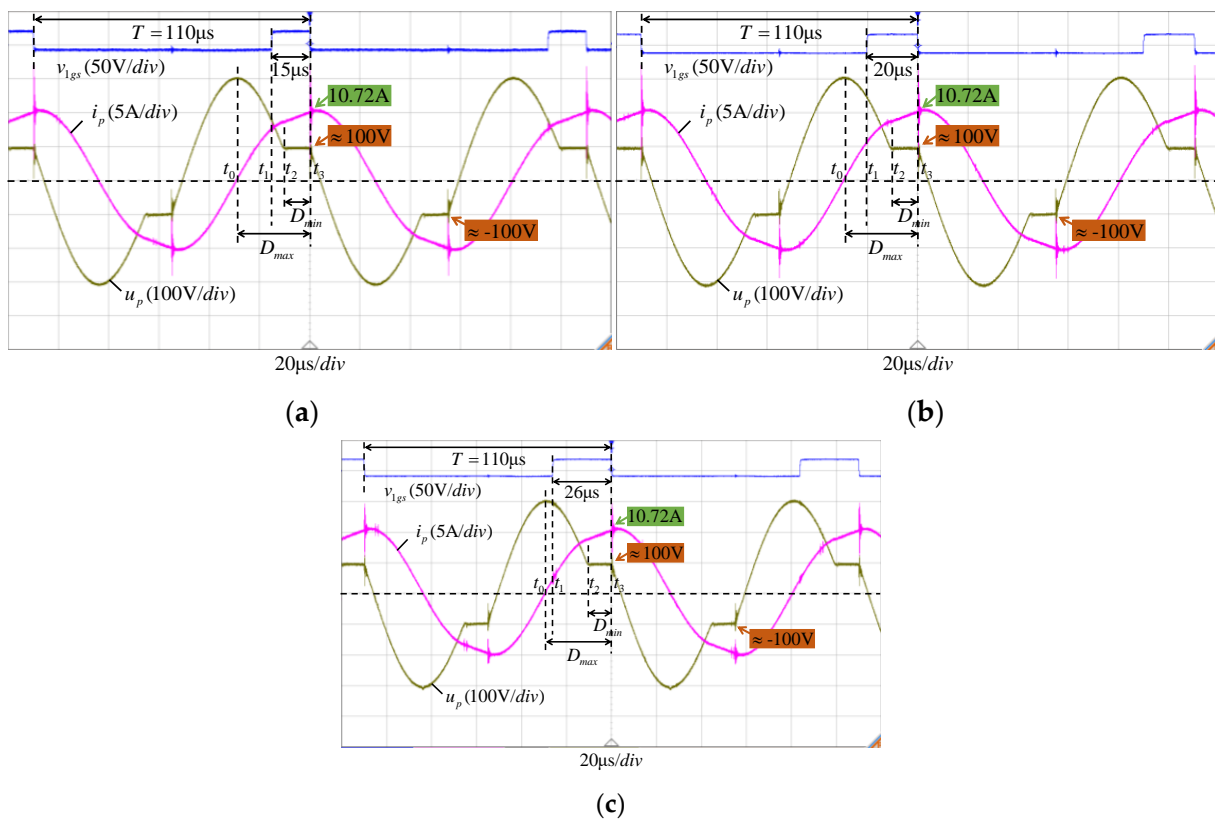


Figure 11. The verification waveforms of the wide soft switching margin: (a) $D = 15 \mu\text{s}$, (b) $D = 20 \mu\text{s}$, and (c) $D = 26 \mu\text{s}$.

3.3. Dynamic Parameter Adaptation Characteristic

The resistance to dynamic parameter changes is a significant dynamic characteristic of WPT systems. Due to no fixed physical connection for wireless coils, environmental disturbances will affect the relative position of the wireless coils to a certain extent, resulting in dynamic changes in the coil coupling coefficient k . On the other hand, a WPT system's equivalent resistance R_L will change as the charging process progresses. Therefore, the coil coupling coefficient k and the equivalent resistance R_L are the main dynamic parameters for research. When the power injection process switches to the free resonance process, the boundary condition depends on the values of the system state variables instead of the switches. The wide soft switching margin characteristic analyzed above, that is, any switching duty $D_1 \in [D_{min}, D_{max}]$ allows the system to operate at $\zeta_1 = D_{min}$, the soft switching operating point. When parameters change dynamically, its soft switching margin has a certain degree of overlap, which can ensure that the system has the characteristics of resisting changes in dynamic parameters, called dynamic parameter adaptive characteristics.

In Figure 12, under the same switching strategy, $T = 110 \mu s$ and $D = 110 \mu s$, there are the curves of M_{ZVS} , D_{min} , and D_{max} concerning the coupling coefficient k . The system parameters are taken according to Table 2, and D_{min} and D_{max} are measured under different k . As seen from Figure 12, in the process of gradually increasing the coupling coefficient k from 0.30 to 0.60, although the soft switching margin has decreased, it has maintained more than 15%.

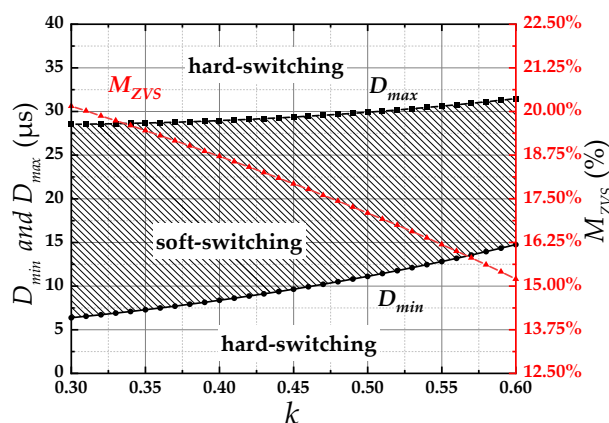


Figure 12. The curves of wide soft switching margin concerning the coupling coefficients k .

Due to the unique hardware structure, the six-switch IPIFR-WPT system can have the ability to dynamically change the coupling coefficient and equivalent load resistance without changing the switching control strategy in the whole process, that is, in the open-loop state.

In the experimental waveforms shown in Figure 13, the switching control strategy of the system is fixed: $T = 110 \mu s$ and $D = 25 \mu s$. Increasing the coil spacing d (a) 6 cm, (b) 7 cm, (c) 8 cm, and (d) 9 cm, the corresponding coupling coefficients k are (a) 0.56, (b) 0.49, (c) 0.43, and (d) 0.38. From the waveforms of the current i_1 , during the process of changing the coupling coefficient k , the system can determine its own soft switching operating point, and its power injection times ζ_1 are self-determined as (a) 12.26 μs , (b) 10.52 μs , (c) 9.26 μs , and (d) 7.86 μs . The waveform trends of the capacitor voltage u_p and the inductor current i_p are always consistent, and the soft switching boundary conditions are satisfied at the boundaries of the free resonance process and the power injection process. In particular, the capacitor voltage u_p can clamp at E_{dc} and $-E_{dc}$ during the power injection process at different coupling coefficients k , which indicates the soft switching conditions have been met. Therefore, this experiment proves that the six-switch IPIFR-WPT system can adapt to the dynamic change of the coupling coefficient k in a great range.

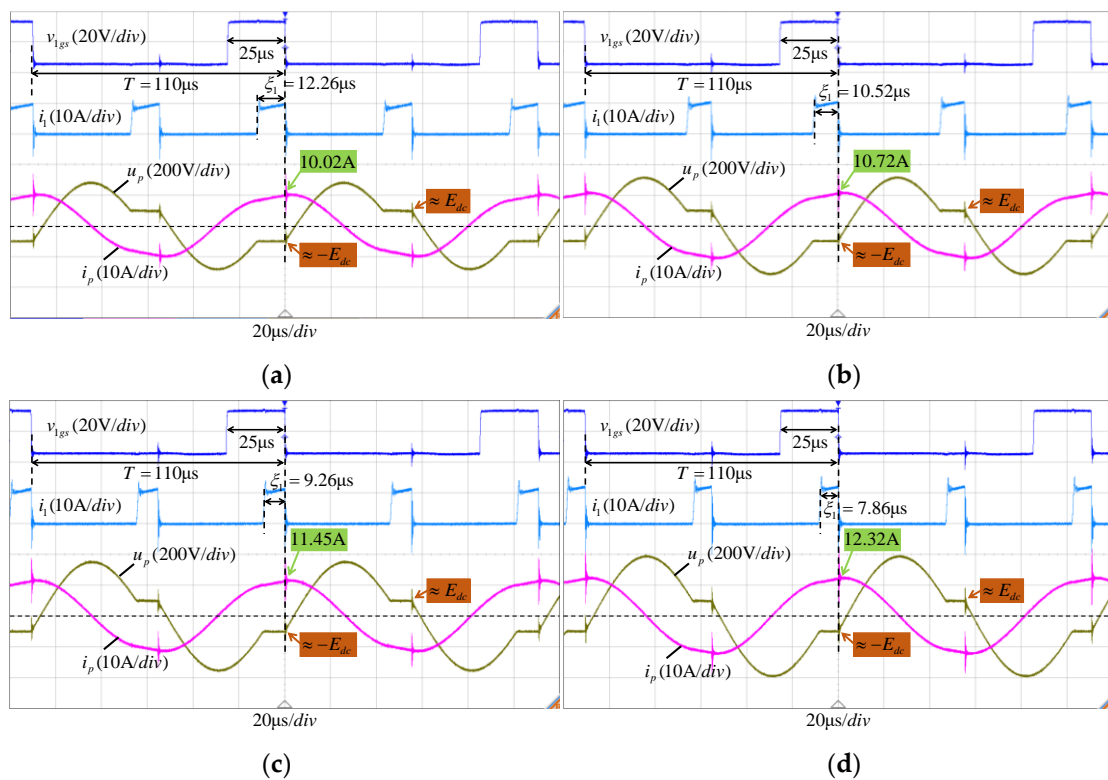


Figure 13. The waveforms of i_1 , i_p , and u_p when coil distance d changes in the open-loop state: (a) $d = 6$ cm, (b) $d = 7$ cm, (c) $d = 8$ cm, and (d) $d = 9$ cm.

Similarly, when the equivalent load resistance R_L changes dynamically, the six-switch IPIFR–WPT system can maintain its adaptive characteristics. As shown in Figure 14, there are curves of the soft switching margin D_{min} and D_{max} concerning the equivalent resistance R_L . In Figure 14, when the equivalent load resistance R_L increases from 5Ω to 20Ω , although the soft switching margin can maintain more than 14%, and when the equivalent load resistance R_L changes in the range of 5Ω to 20Ω , there is a significant overlap range, which allows the system to resist changes in load resistance over a large range.

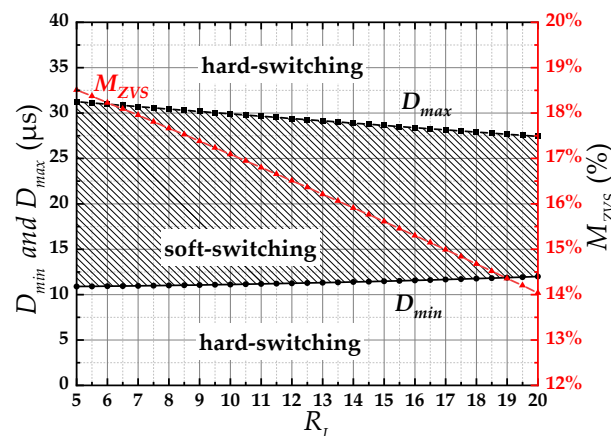


Figure 14. The curves of the wide soft switching margin concerning the equivalent load resistance R_L .

As shown in Figure 15, the switching control strategy of the system is fixed to $T = 110 \mu s$ and $D = 20 \mu s$. When the equivalent load resistances R_L changes, (a) 10Ω , (b) 15Ω , and (c) 20Ω , the waveforms of the current i_1 indicate that the system can determine its own soft switching operating point and power injection times ξ_1 are self-determined as (a) $10.52 \mu s$, (b) $11.29 \mu s$, and (c) $11.94 \mu s$. The waveform trends of the capacitive voltage u_p

and the inductive current i_p are consistent. The larger the equivalent load resistance R_L , the smaller the amplitude of u_p and i_p , indicating that the larger the load resistance, the less energy the system inputs. At the same time, the boundary conditions for switching between the free resonance process and the power injection process can be satisfied. Significantly, the capacitor voltage u_p can be clamped at E_{dc} and $-E_{dc}$ during the power injection process under different equivalent load resistances R_L , which means the soft switching conditions have been satisfied. Therefore, this experiment proves that the six-switch IPIFR–WPT system can adapt to the dynamic changes in the equivalent load resistance R_L over a large range.

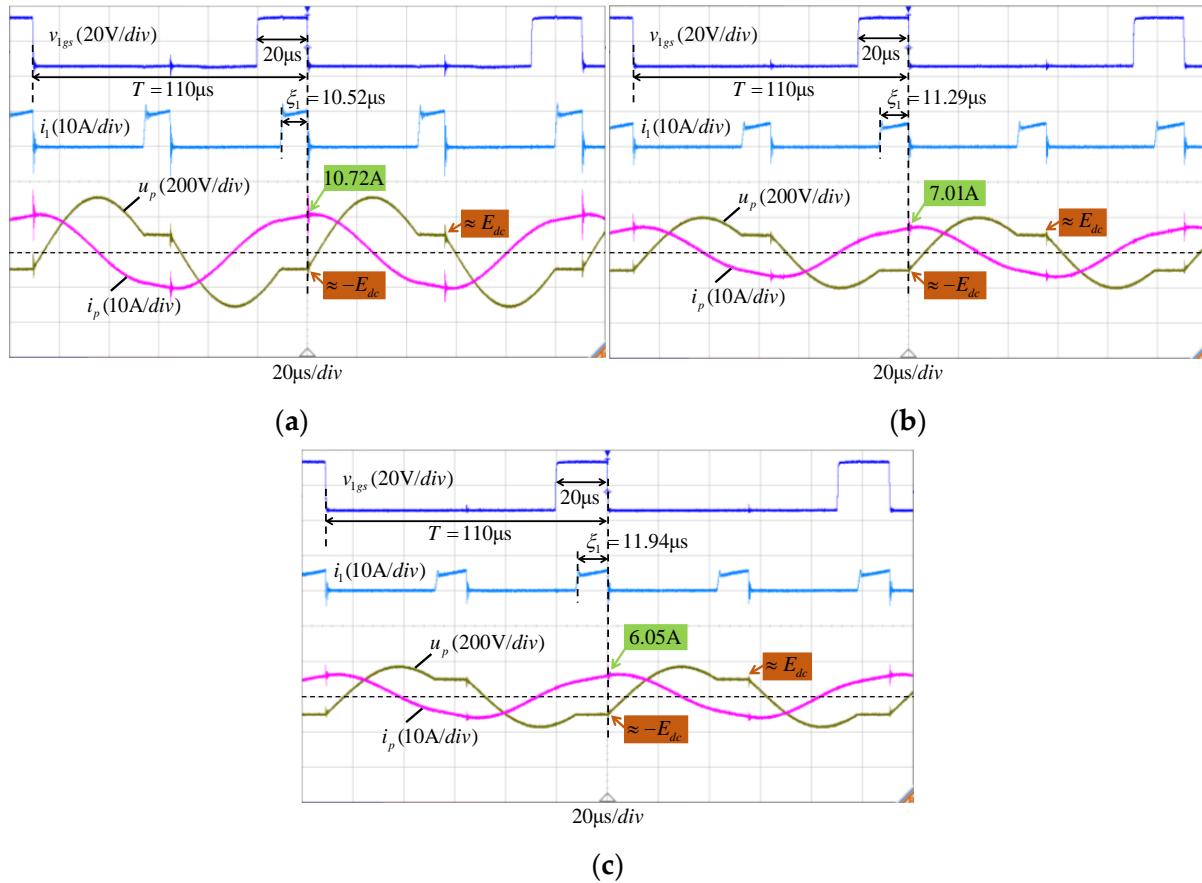


Figure 15. The waveforms of i_1 , i_p , and u_p when load resistance R_L changes in the open-loop state: (a) $R_L = 10 \Omega$, (b) $R_L = 15 \Omega$, and (c) $R_L = 20 \Omega$.

In summary, even in open-loop states, the six-switch IPIFR–WPT system has good adaptability to dynamic changes in parameters such as coupling coefficient k and equivalent load resistance R_L .

3.4. Decoupling Characteristic of Power Injection and Free Resonance

With the changes in T , the curves of the self-determined operating points (ζ_1 , ζ_2) are shown in Figure 16. In Figure 16, as the period T increases, the injection time ζ_1 rises significantly, and ζ_2 remains unchanged, increasing the power injected into the system. Furthermore, due to ζ_2 remaining unchanged, the power injection and free resonance processes exhibit significant decoupling characteristics, which makes the power regulation strategy of the six-switch IPIFR–WPT system extremely simple, that is, directly adjusting the length of the period T .

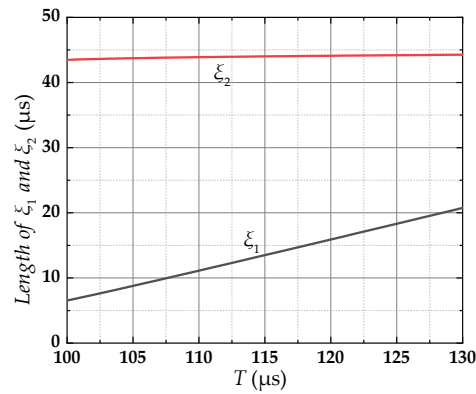


Figure 16. The curves of the self-determining soft switching operation points concerning the period T .

Under static parameters, adjusting the input and output power of the system by changing the length of the period T is actually achieved by changing the power injection time ζ_1 . As shown in Figure 17, when the periods T of the system are (a) 100 μs , (b) 110 μs , (c) 120 μs , and (d) 130 μs , respectively, the determined power injection times ζ_1 are (a) 5.94 μs , (b) 10.52 μs , (c) 13.10 μs , and (d) 20.07 μs . Therefore, as the period T grows, the duration of the power injection time ζ_1 also increases. Meanwhile, the amplitudes of u_p and i_p both increase significantly with the rise of T , meaning the input power increases synchronously.

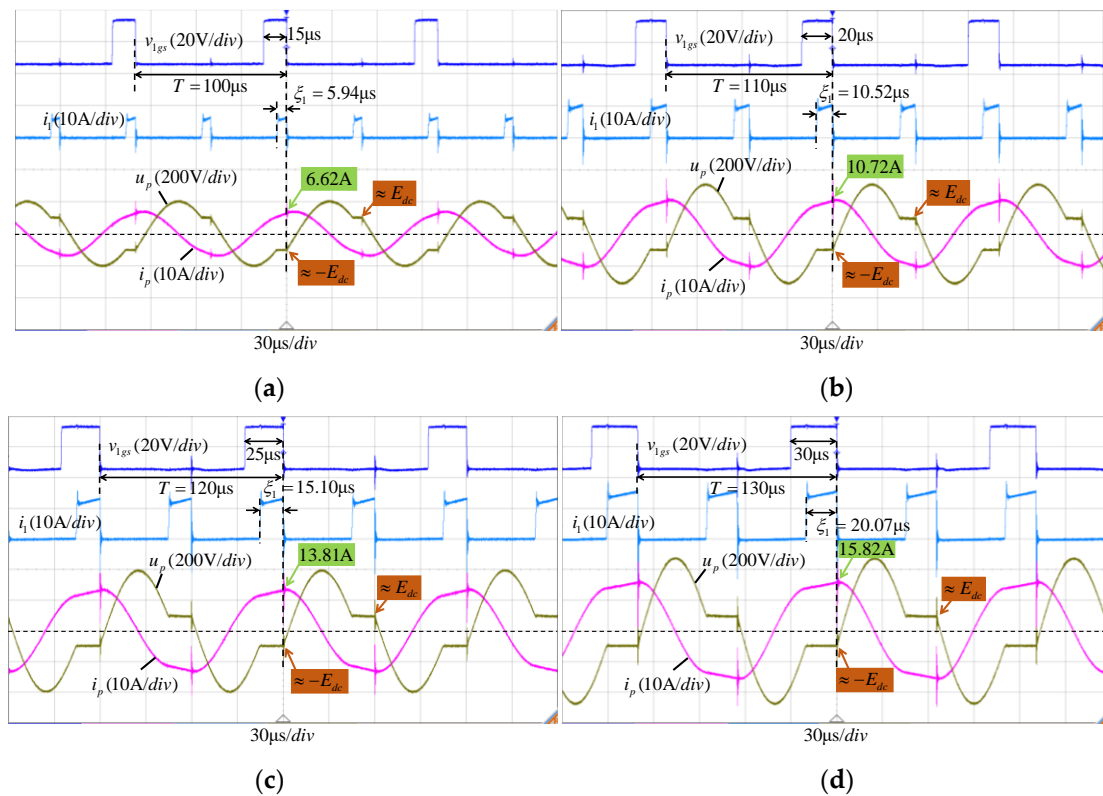


Figure 17. The waveforms of i_1 , i_p , and u_p when T changes in the open-loop state: (a) $T = 100 \mu\text{s}$, (b) $T = 110 \mu\text{s}$, (c) $T = 120 \mu\text{s}$, and (d) $T = 130 \mu\text{s}$.

The calculation methods of the input power P_{in} , the output power P_{out} , and the efficiency η are expressed as follows:

$$P_{in} = E_{dc}I_1, \tag{28}$$

$$P_{out} = \frac{U_{o,rms}^2}{R_L}, \tag{29}$$

$$\eta = \frac{P_{out}}{P_{in}} \times 100\%, \tag{30}$$

where I_1 is the average value of i_{L1} , and $U_{o,rms}$ is the root mean square (RMS) value of u_o .

The curves of the output power P_{out} and the operation efficiency of the six-switch IPIFR–WPT system varying with the period T are shown in Figure 18. It can be seen from Figure 18 that the output power monotonically increases as the period T increases.

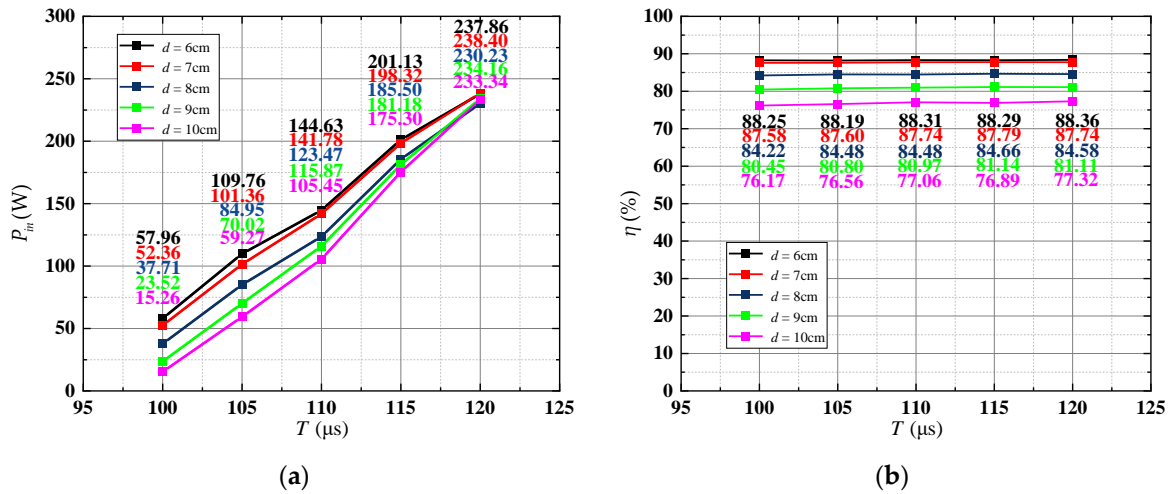


Figure 18. The experimental curves of the output power and efficiency concerning the period T : (a) output power and (b) efficiency.

In Figure 18b, under the same coil spacing d , the operation efficiency of the system remains stable, while with the decrease in coil spacing d , the operation efficiency of the system increases relatively.

In summary, the converter and the resonant network have been decoupled by the unique hardware structures of the six-switch IPIFR–WPT system so that the power injection and the free resonance processes are also decoupled in mode. Under static parameters, the power injected into the system is only determined by the power injection time ζ_1 , and increasing T can make ζ_1 grow, which results in a monotonic relationship between the output power and the period T . Therefore, compared to the fully resonant WPT system, the six-switch IPIFR–WPT system eliminates the peak power point, significantly simplifying power regulation strategies, eliminating system detuning caused by frequency splitting, and improving system stability.

4. Conclusions

This paper completes the theoretical analysis and experimental verification of the dynamic parameter adaptive characteristics and the decoupling of power injection and free resonance in the six-switch IPIFR–WPT system. Firstly, the state space modal is established based on the modal analysis of the six-switch IPIFR–WPT system. Secondly, using the stroboscopic mapping method and boundary conditions, a method is proposed to calculate all possible operating points of the system. Finally, the system characteristics are verified and explained based on simulations and experiments. Unlike traditional FR–WPT systems, the unique topology enables the six-switch IPIFR–WPT system to have adaptive characteristics of dynamic parameters and accomplish decoupling of the power injection and free resonance in modes. The experimental results were consistent with theoretical analysis.

In summary, under open-loop operation states, the unique topology makes the six-switch IPIFR–WPT system have at least 15% and 14% tolerance to the dynamic changes in the coil coupling coefficient k and the equivalent resistance R_L , respectively. Furthermore, the power injection and the free resonance processes are decoupled. Namely, the converter and the resonant network are decoupled. Hence, the power injected into the system is completely controlled, and the curve of output power is monotonic with the injection time ζ_1 or the period T . Moreover, according to the experiments, the power loss is greatest on the coils instead of the diode D_0 . However, in this paper, without precise parameter design, the system efficiency could still achieve 88%.

Furthermore, a suitable parameter design can decrease the internal resistance of coils to improve the system efficiency and reduce the voltage stress to promote the output power.

Author Contributions: Software, W.W.; Formal analysis, W.W.; Resources, W.W.; Data curation, Z.T.; Writing—original draft, W.W.; Writing—review & editing, D.L.; Project administration, D.L.; Funding acquisition, J.H. and W.C. All authors have read and agreed to the published version of the manuscript.

Funding: This research was funded in part by the Natural Science Foundation of China, Grant 52177222, in part by the Natural Science Foundation of Fujian Province, Grant 2021J05262, and in part by the Education Project for Young and Middle aged Teachers of Fujian Provincial Department of Education, Grant JAT200462.

Conflicts of Interest: The authors declare no conflict of interest.

References

1. Zhong, W.; Lee, C.K.; Hui, S.Y.R. General Analysis on the Use of Tesla's Resonators in Domino Forms for Wireless Power Transfer. *IEEE Trans. Ind. Electron.* **2013**, *60*, 261–270. [[CrossRef](#)]
2. He, L.; Guo, D. A Clamped and Harmonic Injected Class-E Converter with ZVS and Reduced Voltage Stress over Wide Range of Distance in WPT System. *IEEE Trans. Power Electron.* **2021**, *36*, 6339–6350. [[CrossRef](#)]
3. Zhang, Z.; Zhang, B. Omnidirectional and Efficient Wireless Power Transfer System for Logistic Robots. *IEEE Access* **2020**, *8*, 13683–13693. [[CrossRef](#)]
4. Zhu, Q.; Wang, L.; Guo, Y.; Liao, C.; Li, F. Applying LCC Compensation Network to Dynamic Wireless EV Charging System. *IEEE Trans. Ind. Electron.* **2016**, *63*, 6557–6567. [[CrossRef](#)]
5. Zhu, Q.; Zhang, Y.; Liao, C.; Guo, Y.; Wang, L.; Li, F. Experimental Study on Asymmetric Wireless Power Transfer System for Electric Vehicle Considering Ferrous Chassis. *IEEE Trans. Transp. Electr.* **2017**, *3*, 427–433. [[CrossRef](#)]
6. Feezor, M.; Sorrell, F.Y.; Blankinship, P.R. An interface system for autonomous undersea vehicles. *IEEE J. Ocean. Eng.* **2001**, *26*, 522–525. [[CrossRef](#)]
7. Lu, Y.; Ma, D.B. Wireless Power Transfer System Architectures for Portable or Implantable Applications. *Energies* **2016**, *9*, 1087. [[CrossRef](#)]
8. Yao, Y.; Wang, Y.; Liu, X.; Lin, F.; Xu, D. A Novel Parameter Tuning Method for a Double-Sided LCL Compensated WPT System with Better Comprehensive Performance. *IEEE Trans. Power Electron.* **2018**, *33*, 8525–8536. [[CrossRef](#)]
9. Huang, R.; Zhang, B.; Qiu, D.; Zhang, Y. Frequency Splitting Phenomena of Magnetic Resonant Coupling Wireless Power Transfer. *IEEE Trans. Magn.* **2014**, *50*, 1–4. [[CrossRef](#)]
10. Huang, R.; Zhang, B. Frequency, Impedance Characteristics and HF Converters of Two-Coil and Four-Coil Wireless Power Transfer. *IEEE J. Emerg. Sel. Top. Power Electron.* **2015**, *3*, 177–183. [[CrossRef](#)]
11. Liao, Z.-J.; Ma, S.; Feng, Q.-K.; Xia, C.; Yu, D. Frequency Splitting Elimination and Utilization in Magnetic Coupling Wireless Power Transfer Systems. *IEEE Trans. Circuits Syst. I Regul. Pap.* **2021**, *68*, 929–939. [[CrossRef](#)]
12. Lim, Y.; Tang, H.; Lim, S.; Park, J. An Adaptive Impedance-Matching Network Based on a Novel Capacitor Matrix for Wireless Power Transfer. *IEEE Trans. Power Electron.* **2014**, *29*, 4403–4413. [[CrossRef](#)]
13. Ann, S.; Lee, B.K. Analysis of Impedance Tuning Control and Synchronous Switching Technique for a Semi-bridgeless Active Rectifier in Inductive Power Transfer Systems for Electric Vehicles. *IEEE Trans. Power Electron.* **2021**, *36*, 8786–8798. [[CrossRef](#)]
14. Wu, M.; Yang, X.; Chen, W.; Wang, L.; Jiang, Y.; Zhao, C.; Yan, Z. A Dual-Sided Control Strategy Based on Mode Switching for Efficiency Optimization in Wireless Power Transfer System. *IEEE Trans. Power Electron.* **2021**, *36*, 8835–8848. [[CrossRef](#)]
15. Namadmalan, A. Self-Oscillating Tuning Loops for Series Resonant Inductive Power Transfer Systems. *IEEE Trans. Power Electron.* **2016**, *31*, 7320–7327. [[CrossRef](#)]
16. Lin, Z.; Wang, J.; Fang, Z.; Hu, M.; Cai, C.; Zhang, J. Accurate Maximum Power Tracking of Wireless Power Transfer System Based on Simulated Annealing Algorithm. *IEEE Access* **2018**, *6*, 60881–60890. [[CrossRef](#)]
17. Luo, D.; Hong, J.; Chen, W. Discrete-Time Modelling to Determine the Possible Operation Points of Incomplete-Resonance Wireless Power Transfer System. *J. Phys. Conf. Ser.* **2022**, *2179*, 012011. [[CrossRef](#)]

18. Chen, L.; Hong, J.; Guan, M.; Lin, Z.; Chen, W. A Converter Based on Independently Inductive Energy Injection and Free Resonance for Wireless Energy Transfer. *Energies* **2019**, *12*, 3467. [[CrossRef](#)]
19. Chen, L.; Hong, J.; Lin, Z.; Luo, D.; Guan, M.; Chen, W. A Converter with Automatic Stage Transition Control for Inductive Power Transfer. *Energies* **2020**, *13*, 5268. [[CrossRef](#)]
20. Wang, Y.; Dong, L.; Liao, X.; Ju, X.; Su, S.W.; Ma, H. A Pulse Energy Injection Inverter for the Switch-Mode Inductive Power Transfer System. *IEEE Trans. Circuits Syst. I Regul. Pap.* **2018**, *65*, 2330–2340. [[CrossRef](#)]
21. Chen, L.; Hong, J.; Guan, M.; Wu, W.; Chen, W. A Power Converter Decoupled from the Resonant Network for Wireless Inductive Coupling Power Transfer. *Energies* **2019**, *12*, 1192. [[CrossRef](#)]
22. Yue, R.; Wang, C.; Li, H.; Liu, Y. Constant-Voltage and Constant-Current Output Using P-CLCL Compensation Circuit for Single-Switch Inductive Power Transfer. *IEEE Trans. Power Electron.* **2021**, *36*, 5181–5190. [[CrossRef](#)]
23. Wang, C.; Yue, R.; Li, H.; Li, D. Research on Constant-Current and Constant-Voltage Wireless Charging System Based on Single-Switch Circuit. *Trans. China Electrotech. Soc.* **2021**, *36*, 4638–4647+4657.
24. Tang, C.S.; Sun, Y.; Su, Y.G.; Nguang, S.K.; Hu, A.P. Determining Multiple Steady-State ZCS Operating Points of a Switch-Mode Contactless Power Transfer System. *IEEE Trans. Power Electron.* **2009**, *24*, 416–425. [[CrossRef](#)]

Disclaimer/Publisher's Note: The statements, opinions and data contained in all publications are solely those of the individual author(s) and contributor(s) and not of MDPI and/or the editor(s). MDPI and/or the editor(s) disclaim responsibility for any injury to people or property resulting from any ideas, methods, instructions or products referred to in the content.